JOURNAL OF APPLIED ELECTROCHEMISTRY **28** (1998) 259–268

A study of current distribution in a DEM cell during bromate formation*

K. SCOTT, W. TAAMA

Chemical & Process Engineering, University of Newcastle, Newcastle upon Tyne, NE1 7RU, Great Britain

B. R. WILLIAMS

ICI Wilton, Middlesbrough, Cleveland, Great Britain

Received 10 February 1997; revised 16 June 1997

The anodic oxidation of potassium bromide to potassium bromate is performed in an undivided cell with hydrogen evolution the major reaction at the counter electrode. The cell used is a dished electrode membrane (DEM) cell. Current density distribution, measured using a segmented electrode, shows a variation in the two principle dimensions; along the length of the electrode and over the width of the electrode. Current densities are highest at the electrolyte flow inlet and also exhibit a localized maximum along the electrode length. The variation in current density is due to the influence of electrolytic gas evolution on the effective electrolyte conductivity and mass transport and also due to the change in shape of the dished electrode, which influences mass transport, electrical potential field and flow at the cell inlet and exit.

Keywords: *bromate*, *anodic oxidation*, *bromine*, *DEM cell*, *current distribution*

List of symbols

C_e	concentration of active species in electrolyte (mol m^{-3})
e	voidage
E_A	anode potential (V)
E_C	cathode potential (V)
E_{cell}	cell voltage (V)
F	Faraday's constant (C mol^{-1})
j_{Al}	partial anode current density (A m^{-2})
j_{Cl}	partial cathode current density (A m^{-2})
j_T	total current density (A m^{-2})
K_e	effective electrolyte conductivity (Ω^{-1} m^{-1})
k_L	mass transfer coefficient (m s^{-1})
M	molar flowrate (mol s^{-3})
V_{SW}	bubble swarm velocity (m s^{-1})
V_g^o	superficial gas velocity (m s^{-1})
V_l^o	superficial liquid velocity (m s^{-1})
Q	volumetric flowrate (m^3 s^{-1})
x	interelectrode gap (m)
y	distance between electrodes (m)
P	pressure (N m^{-2})
r	rate of reaction (mol m^{-3} s^{-1})
R	gas constant (J mol^{-1} K^{-1})
T	temperature (K)
Sc	Schmidt number
Sh	Sherwood number
Re	Reynolds number

Superscripts and subscripts

g	gas
s	surface
m	mesh

1. Introduction

The generation of gas bubbles by electrochemical reactions has a significant effect on electrochemical reactor operation. The production of bubbles at electrode surfaces will influence mass transport at the surface, generally increasing mass transfer rates, above that obtained in the absence of gas evolution, due to an increase in the fluid turbulence. Gas bubbles will increase the effective resistivity of the electrolyte in the locality of the electrode surface and will also cause a bubble overpotential. The movement of gas bubbles into the bulk of the electrolyte will increase the electrolyte conductivity in that region and will influence mass transport at the counter electrode through turbulence promotion. Overall gas bubble generation is likely to have a considerable effect on fluid flow and mixing, on mass transport of ionic species and on current distribution. The effect of gas bubbles on mass transfer in electrochemical reactors has been studied in several situations [1, 2]: (i) at gas evolving electrodes, (ii) at working electrodes in the presence of gas sparging to create bubbles, and (iii) at working electrodes in the presence of gas generating

* This paper was presented at the Fourth European Symposium on Electrochemical Engineering, Prague, 28–30 August 1996.

electrodes. These studies were conducted with and/or without superimposed electrolyte flow, (iv) at working electrodes with gas bubbles produced at the counter electrode [3–5]. Mass transfer has been studied at various electrode systems; at vertical gas evolving electrodes [6–9], at horizontal electrodes [10, 11], at the gas evolving inner electrode of a concentric cylindrical reactor [12] and in the presence of gas sparging [13]. A number of models have also been proposed for mass transfer at gas evolving electrodes [14–16]. However, only limited results are available in the literature concerning mass transfer enhancement, due to gas generated at counter electrodes.

Current distribution in electrochemical reactors with parallel plate electrodes has been extensively studied [17–25] and models have been developed for monopolar electrochemical reactors [20–22]. Bisang has reported theoretical and experimental studies of current distribution in a monopolar reactor with gas evolving electrodes [23]. More recently the distribution of current density has been measured and modelled during the anodic oxidation of sulphite to sulphate in basic solution [26]. Significant nonuniform current distribution was found, associated with the interaction of gas induced mass transport, bubble flow and effective electrolyte conductivity.

The present work is concerned with the study of the current distribution in a dished electrode membrane (DEM) cell used for the production of sodium bromate by anodic oxidation of bromide during undivided cell electrolysis. The concept of the DEM cell (shown in cross section in Fig. 1 and in detail in Fig. 2) is to utilize a dished electrode to achieve a small interelectrode gap whilst retaining a relatively thick electrolyte frame to enable simple connection of external pipework. The synthesis of sodium bromate from sodium bromide is of some commercial interest and there have been a number of studies of the process [27, 28]. The production of sodium bromate in a DEM cell has been the subject of a mathematical reactor model [29]. This model did not account for any current distribution over the electrodes associated with variations in mass transport and conductivity although this was identified as a factor in explaining differences in current efficiency on scale-up. Consequently, this study was undertaken to both measure the current distribution in the DEM cell during the anodic formation of bromate and to incorporate this factor in a mathematical model. The design concept of the DEM cell is to achieve a small interelectrode gap in a relatively large electrolyte compartment frame. The dishing of the electrodes means that at the periphery of the electrode there is a geometric effect introduced which influences current distribution, fluid flow and mass transport.

2. Experimental system

The current work used a small pilot scale undivided DEM cell. The cell consisted of one frame, made from u-PVC, with an overall size of 0.35 m × 0.35 m × 0.026 m, between a flat electrode and a dished electrode. The anode was a sheet DSA electrode (with an active area of 0.28 m × 0.28 m) and the dished cathode was stainless steel; segmented to allow the current distribution to be measured (Fig. 3). Overall there were 25 electrode segments, 56 mm × 56 mm in cross section, arranged in five rows and five columns. The central nine segments were flat, the remainder were shaped to the contour of the dished electrode. A turbulence promoter made of Netlon® PVC mesh was used to promote uniform flow. The pipework for electrolyte flow to the cell was located at the bottom and top sides of the cell frame. There two flow inlets and two flow outlets were positioned at the corner segments of the cathode (Fig. 1). Provision was made for the introduction of fine bore (1 mm) plastic coated, stainless steel capillary tubes through the cell frame to measure local electrode potentials. The cell was located in a batch recirculation flow rig with electrolyte circulated, from a polypropylene tank (20 dm^3 capacity), by a magnetically driven pump. To prevent vortex formation at high

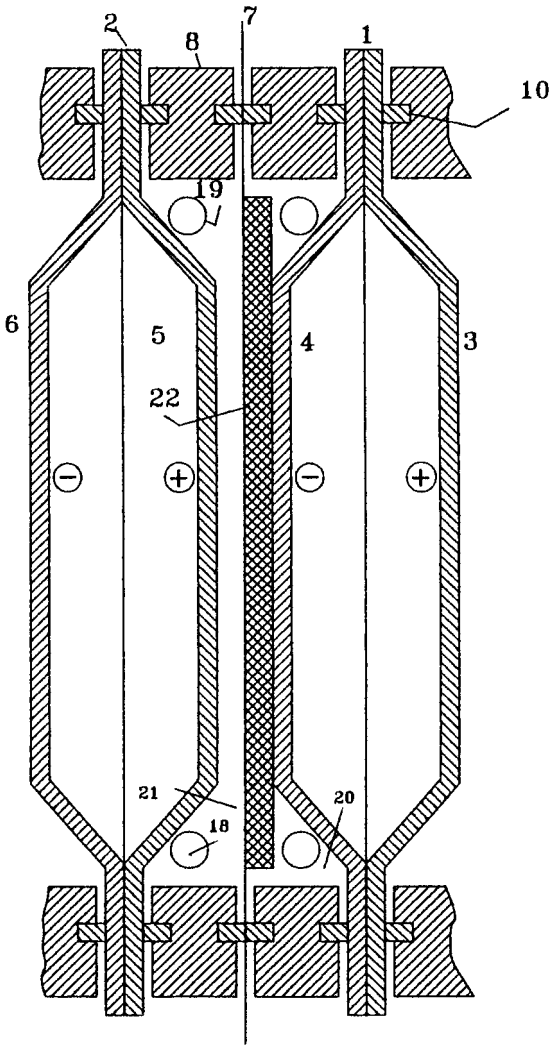

Fig. 1. Cross section through DEM cell. Key: (1, 2) dished electrodes, cathode surfaces; (3, 5) cathode surfaces; (4, 6) anode surfaces; (7) cell divider; (8) frame members; (10) sealing ring; (18) inlet port; (19) outlet port; (20, 21) individual compartments; (22) turbulence promoter.

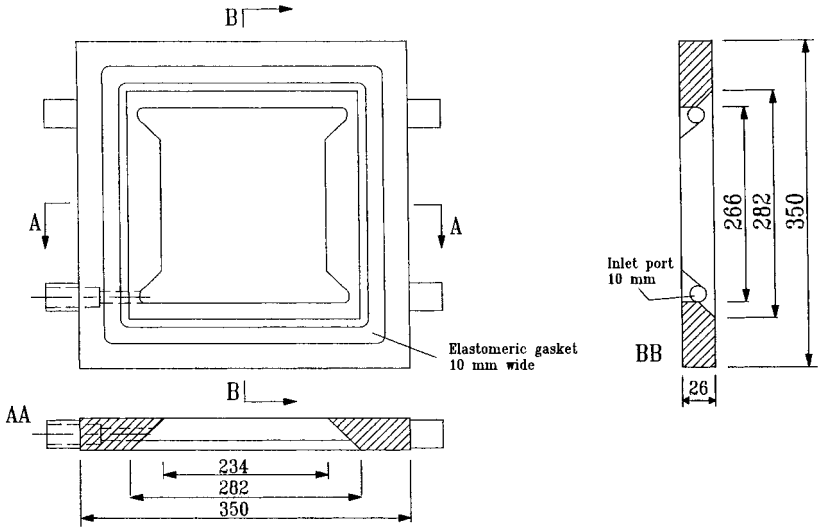

Fig. 2. Cell frame geometry. All dimensions are in millimetre.

flowrates, a polypropylene baffle/weir was positioned near the outlet of the tank. Recirculating electrolyte flowed through glass wool in the tank to disengage electrochemically generated gas bubbles. As a result of the batch recirculation operation, the electrolyte was saturated with evolved gas and contained a very small fraction of dispersed fine gas bubbles. Electrolyte temperature was maintained at approximately 30 °C (±1 °C) using a glass coil heat exchanger. The cell power was supplied by an 80 A regulated d.c. power supply (Farnell). To measure the currents through each segment of the cathode, a 0.01 Ω resistor was connected in series with each segment. The voltage across each resistor was amplified to provide an input to an analogue to digital converter which was part of a pc30-AT data acquisition board. Electrolyte solutions were made from Analar grade (BDH) potassium bromide in deionized water.

3. Mathematical model

The system under study is considered to be an undivided plate electrolyser in which the anodic oxidation of bromide ions takes place. Hydrogen gas is evolved at the cathode and the resulting gas bubbles are uniformly distributed between the electrodes (see Fig. 4). The reaction under study was the electrolysis of potassium bromide solution to produce potassium bromate by the following series of reactions:

at the anode:

$$2Br^- = Br_2 + 2e^- \tag{1}$$

at the cathode:

$$2H_2O + 2e^- \longrightarrow H_2 + 2OH^- \tag{2}$$

in the solution:

$$Br_2 + H_2O == HOBr + H^+ + Br^- \tag{3}$$

$$HOBr = OBr^- + H^+ \tag{4}$$

$$Br_2 + Br^- = Br_3^- \tag{5}$$

$$OBr^- + 2HOBr \longrightarrow BrO_3^- + 2H^+ + 2Br^- \tag{6}$$

Reaction 5 is an equilibrium process which affects the available bromine for the hydrolysis, Reaction 3, to hypobromous acid. In addition, two electrode reactions which cause a reduction in current efficiency are considered;

at the anode:

$$6\,OBr^- + 3\,H_2O \longrightarrow 2\,BrO_3^- + 4\,Br^- + 6\,H^+ + 3/2O_2 + 6\,e^- \tag{7}$$

at the cathode:

$$OBr^- + H_2O + 2e^- \longrightarrow Br^- + 2OH^- \tag{8}$$

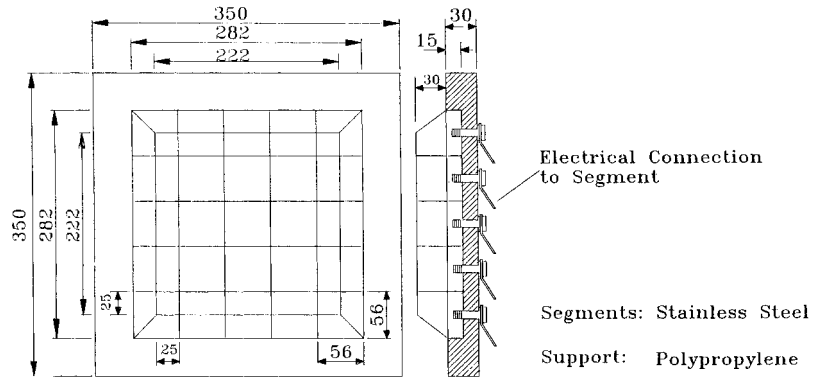

Fig. 3. Segmented electrode system of the DEM cell.

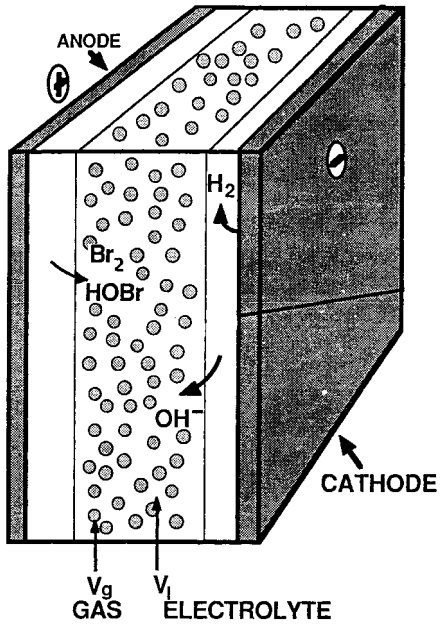

Fig. 4. Schematic diagram of the parallel plate electrolyser.

It should be noted that Reaction 7 leads to a loss of current efficiency, since it consumes hypobromite ions which would otherwise react chemically to form bromate. The kinetic and equilibrium data for these reactions, have been summarized by Cettou [30]. The pH of the electrolyte varied between 8 and 12 during an experiment to favour rapid bromine hydrolysis. In addition to the reaction of the bromide species, evolution of oxygen due to the electrolysis of water could also occur at high current densities.

The mathematical model is developed to determine the one dimensional distribution of current density along the length of the electrode, associated with variations in effective electrolyte conductivity, mass transport and reaction species concentration. The overall voltage, E_{cell}, is written as the sum of the voltage drop in the electrolyte phase and the anode and cathode potentials E_A and E_C.

$$E_{\text{cell}} = E_A - E_C + j_T x/K_e = \text{constant} \qquad (9)$$

where j_T is total current density, x the interelectrode gap and K_e effective electrolyte conductivity.

The following main assumptions are used in the model: (i) in the solution phase the current flows in a direction normal to the electrode surface; (ii) the reversible cell potentials are not a function of the electrode position; (iii) ohmic voltage losses in the electrode are negligible; (iv) the reactor is isothermal; and (v) the distribution of bubbles is uniform over the width and thickness of the cell.

Since it has been assumed that the current flows normal to the electrodes at all points, then the total current density, j_T, will be the same at opposite points on the electrodes. At the anode, two reactions are considered. The desired anode reaction is the oxidation of bromide ions to bromine. In addition, some hypobromite ions are oxidized to form bromate, in a loss reaction. Similarly two reactions are considered at the cathode. The desired reaction is hydrogen evolution and the loss reaction is the reduction of hypobromite ions. Thus the overall current balance is

$$j_T = j_{A1} + j_{A2} = j_{C1} + j_{C2} \qquad (10)$$

where j_{A1} is the partial current density for the oxidation of bromide, j_{A2} the partial current density for the oxidation of hypobromite assumed to be mass transfer limited, j_{C1} the partial current density for hydrogen evolution and j_{C2} the partial current density for the reduction of hypobromite ions, assumed to be mass transfer limited.

The values of j_{A1} and j_{C1} are given by the following Tafel equations determined from separate experiments in a small glass laboratory cell:

$$j_{A1} = 1.585 \times 10^{-7} C^{s}_{Br^-} \exp[0.229\, zFE_A/RT] \qquad (11)$$

$$j_{C1} = 3.738 \times 10^{-11} \exp[-0.162\, zFE_c/RT] \qquad (12)$$

where $C^{s}_{Br^-}$ is the concentration of bromide ion at the electrode surface.

Measurement of polarization behaviour in the DEM cell using fine capillary tubes gave reasonable correspondence with these values. The effective electrolyte conductivity allows for the influence of the gas bubbles and the Netlon® mesh on the actual electrolyte conductivity. The overall effective conductivity, K_e, was expressed in terms of the Bruggeman equation:

$$K_e = K[1 - e]^{-1.5} \qquad (13)$$

where K is the single phase electrolyte conductivity and e the overall voidage, given by

$$1 - e = (1 - e_m)(1 - e_g) \qquad (14)$$

e_m is the voidage of the Netlon mesh and e_g the gas voidage given generally by the Kreysa and Kuhn relationship.

$$\frac{1}{e_g} = \frac{1}{e_l} + \frac{V_l^o(1 - e_g/e_m)}{V_g^o(1 - e_g)} + \frac{V_{SW}}{V_g^o} \qquad (15)$$

where e_l is the limiting gas voidage, V_l^o and V_g^o are superficial liquid and gas velocities respectively and V_{SW} is the bubble swarm velocity given by

$$V_{SW} = V_s(1 - e_g)^{4.5} \qquad (16)$$

where V_s is the rise velocity of a single bubble.

The gas velocity, V_g^o, is predominantly due to hydrogen and is given by

$$V_g^o = \frac{RT}{Pv_cFx}\int_0^y j_{C1}\, dy \qquad (17)$$

where v_c is the charge number.

The model requires correlations for mass transport at the electrode surface. The mass transfer coefficient for single phase flow, k_{LS}, has been correlated for the DEM cell by Taama [31]. Entrance and exit effects may be adequately accounted for by using three separate correlations for the bottom, top and central rows of the segments as follows:

Central region

$$Sh = 0.502\, Re^{0.489}\, Sc^{0.33} \qquad (18a)$$

Top row

$$Sh = 0.234\, Re^{0.534}\, Sc^{0.33} \qquad (18b)$$

Bottom row

$$Sh = 0.832\,Re^{0.418}\,Sc^{0.33} \tag{18c}$$

The presence of gas bubbles in the electrolytes is expected to radically influence the mass transfer characteristics at the electrode. The effect of gas bubble generation will in turn be influenced by the change in shape of the DEM cell electrodes at inlet and exit. Mass transfer characteristics at the flat electrode will be different to those at the dished electrode and will additionally depend upon which electrode is responsible for gas (hydrogen) evolution. This mass transfer behaviour is complex and is not known for the DEM cell. Thus in this model we use correlations from previous studies which describe the effect of gas bubbles generated at the counter electrode on mass transfer at the working electrode. The generation of hydrogen gas at the cathode also influences the mass transfer characteristics at this electrode. This will influence the rate equations for hydrogen evolution and for the reduction of hypobromite ions. A correlation describing the effect of bubbly flow on the mass transfer coefficients has been reported [32] for a cell design without a turbulence promoter, that is,

$$k_L = k_{LS} + a\,v_L^b v_G^c \tag{19}$$

where k_L is the two phase mass transfer coefficient and k_{LS} the single phase mass transfer coefficient.

The coefficients a, b and c are 1.11×10^{-4}, 0.74 and 0.36, respectively. This correlation is used in the first instance to estimate the influence of mass transport on the reaction rates.

The mass transport correlations are used to determine the rate (current density) of the mass transport controlled loss reactions in the overall reaction system and to calculate the surface concentration of bromide ions in the main anodic reaction, the generation of bromate. To complete the model a series of component material balances are used to enable distributions of concentration along the length of the electrode to be computed:

$$\frac{dM}{dV_n} = \frac{1}{Q}\frac{dM}{dt} - r \tag{20}$$

where M is the molar flowrate of species in the electrolyte, dV_n the volume of incremental element, Q the volumetric flowrate and r the rate of reaction of species. The appropriate rates of reaction are given in Table 1 for all the species. All nonelectrochemical reactions are assumed to be homogeneously distributed in the bulk electrolyte. The model was solved using a dynamic simulation package (SPEEDUP™ from Aspen).

4. Experimental results

The pipework connections to the DEM cell are located at the bottom and top sides of the cell frame. These connections cause nonuniform flow inside the DEM cell and, correspondingly, mass transport will be nonuniform [31], particularly in an empty channel cell. Consequently all experiments were performed with two sheets of Netlon® mesh exactly filling the interelectrode gap. Even with turbulence promoting mesh the flow through the cell is still expected to be nonuniform, with flow at the inlet tending to channel towards the centre line of the cell. An additional practical feature of the cell which affects current distribution is that the inlet and exit flows to opposite sides of the cell are from, and to, T-junctions in a common pump line. Thus any imbalance in pressure after the T-junction splits the flow, will affect the relative flows into each line to the cell which in turn will influence the current distribution across the width of the cell. Although this effect was minimized, it was still apparent in some of the current density distribution data collected.

Figure 5 shows a typical distribution of current density along each row of the segmented electrode. Generally current density is slightly higher at the outer electrode segments. This is largely due to the position of the flow inlet to the cell, which along with the interactive effects of gas evolution, electrolyte conductivity and mass transport produces a rather

Table 1. Rates of reaction in the production of bromate

Reaction	*Rate of Production*/kmol m^{-3} s^{-1}									
	Br^-	Br_2	H_2	OH^-	BrO^-	BrO_3^-	Br_3^-	H^+	O_2	$HOBr$
1	$-\sigma i_l/F$	$\sigma i_{Al}/2F$								
2			$\sigma i_{Cl}/2F$	$\sigma i_{Cl}/F$						
7	$2\sigma k_l C_{OBr^-}/3$				$-\sigma k_l C_{BrO^-}$	$\sigma k_l C_{OBr^-}/3$		$-\sigma k_l C_{BrO^-}$	$\sigma k_l C_{OBr^-}/4$	
8	$\sigma k_l C_{BrO^-}$			$2\sigma k_l C_{BrO^-}$	$-\sigma k_l C_{BrO^-}$					
4					$R_{hydrogen}$			$R_{hydrogen}$		$R_{hydrogen}$
5	$-R_{tribromide}$	$-R_{tribromide}$					$-R_{tribromide}$			
6	$2k_3 C_{HOBr}^2$				$-k_3 C_{HOBr}^2$			$2k_3 C_{HOBr}^2$		$-2k_3 C_{HOBr}^2$
	$^*C_{OBr^-}$				$^*C_{OBr^-}$			$^*C_{OBr^-}$		$^*C_{OBr^-}$
3	$k_1 C_{Br_2}$	$k_2 C_{HOBr}$						$k_1 C_{Br_2}$		$k_1 C_{Br_2}$
	$-k_2 C_{HOBr}$	$^*C_{H^+} C_{Br^-}$						$-k_2 C_{HOBr}$		$-k_2 C_{HOBr}$
	$^*C_{H^+} C_{Br^-}$	$-k_1 C_{Br_2}$						$^*C_{H^+} C_{Br^-}$		$^*C_{H^+} C_{Br^-}$
9				R_{water}				R_{water}		

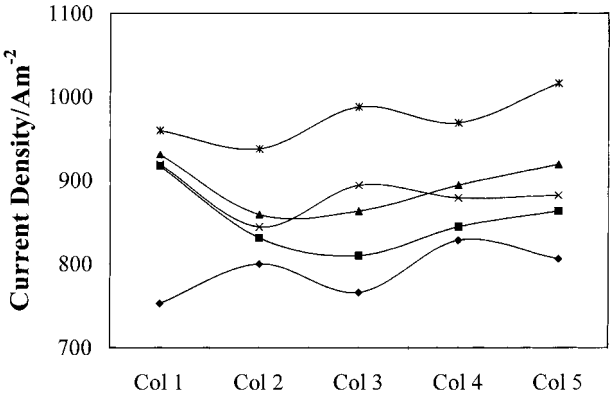

Fig. 5. Current distribution over the segmented electrode. Key: (◆) row 1 (top); (■) row 2; (▲) row 3; (×) row 4; (∗) row 5.

complex current distribution, even on a macro-scale level measured with only 25 segments. A notable feature of all the data in Fig. 5 is that, in each column of segments, current density is always the greatest at the bottom of the cell (flow inlet, row 5), and is lowest at the top of the cell. However, in the central column, the current density distribution exhibits a secondary maximum in the centre row, 3. It is interesting to consider how this effect may arise. A high current density at the inlet can be associated with a high effective electrolyte conductivity, a low bubble fraction and a high mass transfer rate due to a large flow inlet effect. The continuous decrease in current density along the centre column segments indicates that the effective conductivity of the electrolyte is falling due to an increase in the entrained gas (H_2) fraction. The electrolyte flow in the centre column of the cell is expected to be relatively low, again due to the position of the flow inlets and exits, and thus mass transfer enhancement due to gas bubbles will not be as high as elsewhere in the cell. The dominant factor, other than the inlet effect, which determines the current density is thus the effective conductivity. This is reflected in the current density data in the centre top segment which always exhibits the lowest current density of all the segments. A secondary feature at the flow exit could be the influence of a relatively high gas fraction due to gas swirling associated with vortex flow. At the outer column segments, electrolyte flow is potentially greater than in the centre and thus mass transfer enhancement is greater, whilst effective conductivity is also greater (smaller relative gas fraction), and thus the possibility of a local maximum in current density exists in theory.

In this study we considered the influence of electrolyte flowrate, overall current density and electrolyte concentration on the current density distribution to explore the interactive effects of mass transport and effective conductivity. The current densities were chosen to give a mixed kinetic and mass transport control for bromide ion oxidation. Figure 6 summarizes current density distribution data for two flowrates in the cell, with total currents of 40 to 80 A and electrolyte concentrations of 1.0 and 1.5 M. All the data show the same characteristic of the highest current density at the cell inlet and lowest current density at the cell exit. The variation in current density from inlet to exit is greater at the highest cell current, varying by approximately ±20% from the mean current density applied. The influence of electrolyte concentration on the current density distribution is not great, except near to the cell inlet and with a low flowrate.

Typical data on the effect of flowrate on the average current density along each row of segments is shown in Fig. 7. The data generally exhibit a localized maximum in current density at row 3. With a 1.5 M KBr electrolyte the data show that, at each current applied, the current density at the cell inlet row of segments (5) increases as the flowrate decreases. This behaviour is probably associated with greater gas bubble fractions at the lower flowrates, coupled with a significant flow inlet effect, which can increase the mass transfer rate and which consequently reduces the 'effective electrode polarization resistance' and thus increases the current density. At the segments at the cell exit, at each current applied, the effect of flowrate on current density is not as significant as at the cell inlet. Only at the highest flowrate used is there a significant change in current density. In this case the current density has its highest value at the highest flowrate. This apparent reversal of behaviour at the cell exit is probably due to the higher gas bubble fractions experienced at the exit. There is thus probably quite different mass transfer behaviour at the cell exit and in addition a high flowrate will reduce the effective electrolyte resistance and thus will tend to increase the current density.

The effect of flowrate on the current density distribution is different with a 1.0 KBr electrolyte than with a 1.5 M KBr electrolyte (Fig. 7). The aforementioned decrease in current density with increase in flowrate is only seen at the lower current applied (i.e., 40 A). At the higher overall currents applied, 60 A and 80 A (not shown), the current density at the row of segments at the cell inlet increases as the flowrate increases. This overall change in current density distribution behaviour is due to the relative influence of flowrate on the mass transfer behaviour and on the effective electrolyte conductivity. The electrolyte conductivity of a 1.0 M KBr solution is lower than that of a 1.5 M KBr solution, which means that the effective electrolyte conductivity will play a greater role in determining the current density distribution with a 1.0 M KBr electrolyte than with a 1.5 M KBr electrolyte. In addition as the current is increased the gas bubble fraction increases, leading to a decrease in effective conductivity. Therefore under conditions when the cell voltage contribution associated with the electrolyte resistance is more significant, that is, with a 1.0 M KBr electrolyte, a higher flowrate will tend to reduce the effective resistance by reducing the overall gas fraction.

Figure 8 shows the typical variation in cell voltage with electrolyte flowrate for this reactor. A change in flowrate from 41 $cm^3 s^{-1}$ to 298 $cm^3 s^{-1}$ causes a re-

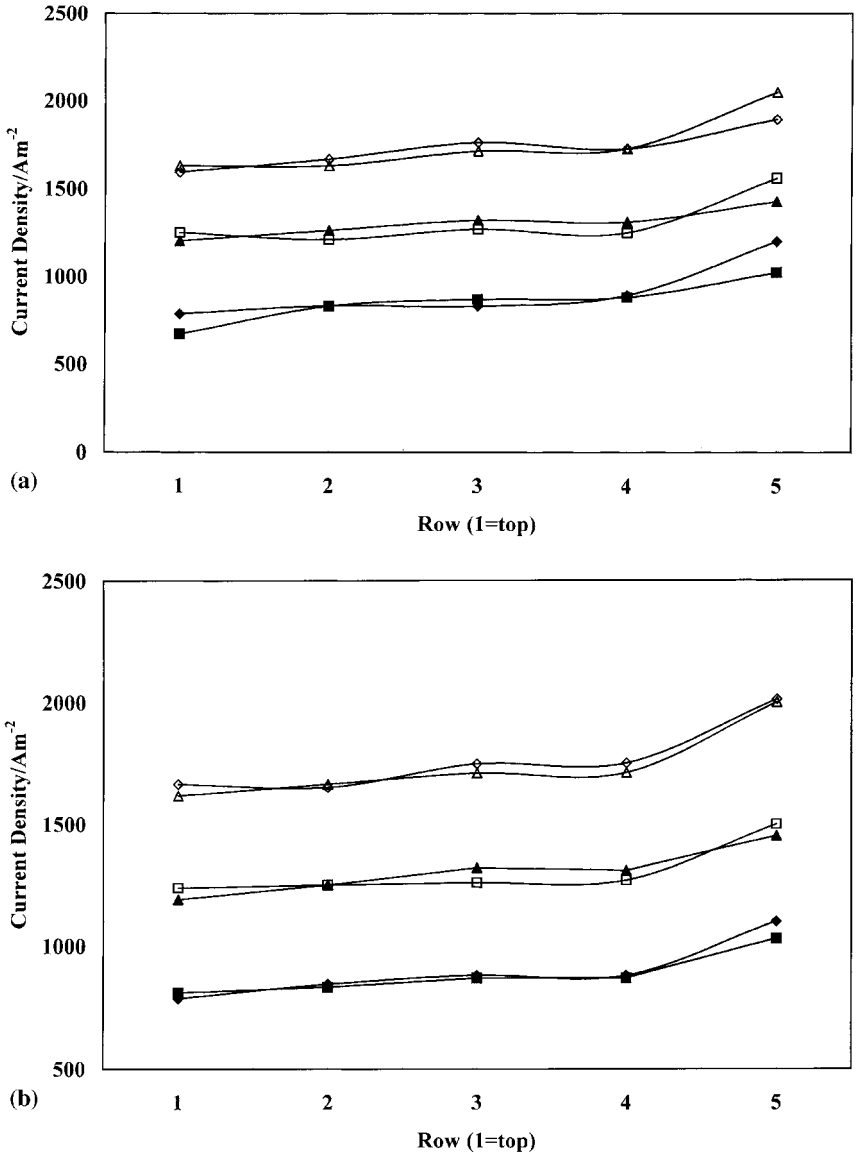

Fig. 6. Effect of electrolyte concentration on current distribution. Key: (■) 40 A, 1.0 M, (◆) 40 A, 1.5 M, (▲) 60 A, 1.0 M, (□) 60 A, 1.5 M, (◇) 80 A, 1.0 M, (△) 80 A, 1.5 M. Flow rate: (a) 96 and (b) 298 $cm^3 s^{-1}$.

duction in voltage of between 100 to 350 mV (80 A, 1.5 M KBr). This voltage reduction is a combined effect of an increased effective electrolyte conductivity (reduced bubble voidage) and possibly an increase in mass transfer rate at the higher Reynolds number. However, it might be expected that a reduced bubble voidage would reduce mass transport rates as the turbulence promoting effect is reduced. However, it is uncertain whether this would be the case in the presence of a turbulence promoting mesh. Similar measurements of the effect of liquid–liquid dispersions on mass transport have noted only a small influence of liquid dispersion void fraction on the mass transport rates. From the cell voltage data of Fig. 8, it would appear that a major factor is the effect of gas bubble voidage on the effective conductivity. In the absence of a variation in mass transport along the electrode it would be expected that current density would decrease from inlet to exit, which is indeed observed for the central column of electrode segments.

5. Discussion

Overall the experimental data show that current density is significantly greater at the cell inlet than elsewhere in the reactor. Qualitatively this behaviour corresponds to a lower effective electrolyte resistance and to lower effective electrode reduced polarization. In addition, the current density distribution, when averaged for each row, exhibits a localized 'maximum' beyond the inlet section. This latter behaviour corresponds to the case where (a) nearer the inlet, mass transport is relatively low and approaches a localized minimum as observed in cells with counter electrode gas evolution in the absence of turbulence promoter. Such cells also exhibit significant mass transport entry effects; and (b) further along the electrode mass transport increases and the major cause of the reduced current density is the lower effective electrolyte conductivity.

The ability of the model to predict the localized distribution in current density is demonstrated in

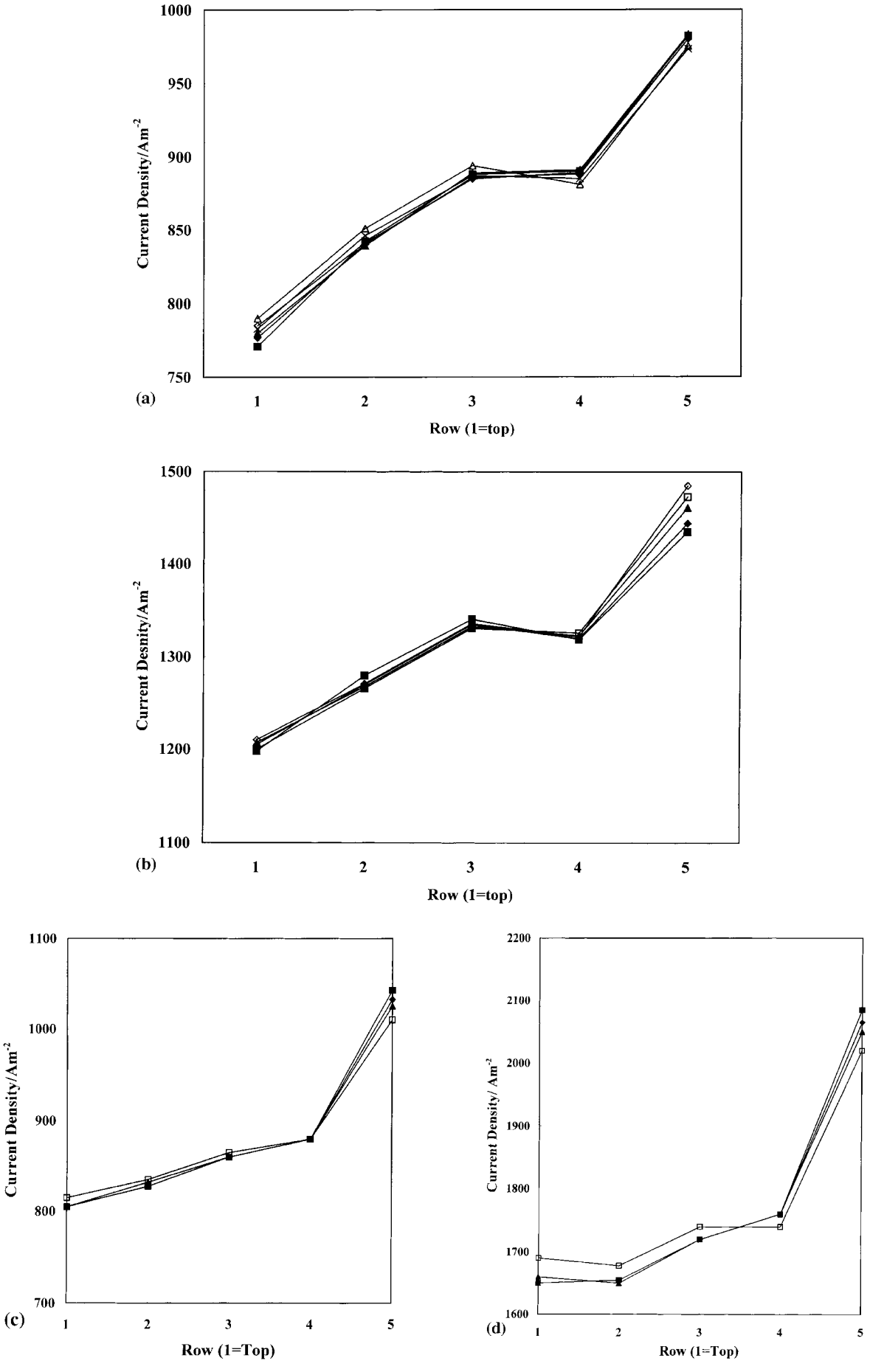

Fig. 7. Effect of flowrate on the average distributions of current density along the DEM cell. (a) 1.0 M KBr, 40 A. (b) 1.0 M KBr, 60 A. Key to flowrate/cm^3 s^{-1}: (■) 41, (◆) 60, (▲) 96, (□) 160, (◇) 227, (△) 298. (c) 1.5 M KBr, 40 A. (d) 1.5 M KBr, 40 A. Key to flowrate/cm^3 s^{-1}: (■) 60, (◆) 96, (▲) 100, (□) 298.

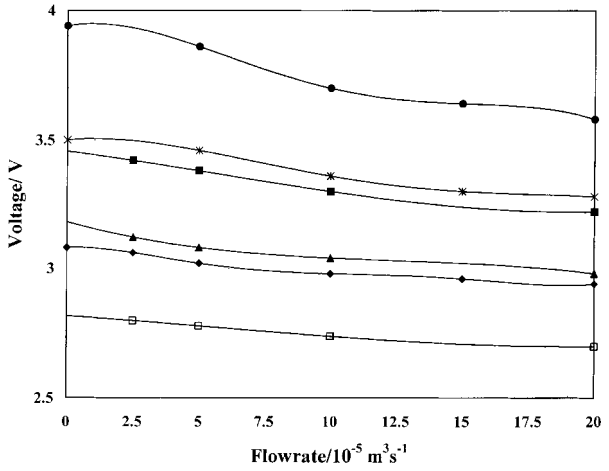

Fig. 8. Variation of cell voltage with flowrate. Key: (◆) 40 A, 1.0 M, (∗) 60 A, 1.0 M, (●) 80 A, 1.0 M, (□) 40 A, 1.5 M, (▲) 60 A, 1.5 M, (■) 80 A, 1.5 M.

Fig. 9. The model does not predict the higher current density at the cell inlet which is associated with a high mass transport entry effect. This entry effect is accentuated by the dished shape of the segment at the point of flow entry. The dished electrode causes a change in the mean flow path around the edge of the electrode and also the mesh turbulence promoter is not in contact with approximately half of the electrode segment due to the change in shape. A major factor is that at the flow inlet and exit regions there is a change in the effective interelectrode gap due to the dishing of the electrode and that the dished electrode does not completely fill the cross section of the cell, that is, there is an edge effect which could invalidate the assumption of the current flow being everywhere normal to the electrode surface. In other words, in terms of pure primary current distribution, there could be higher current densities at the ends of the electrodes than in the remaining sections.

If the variation in current density at the ends of the electrodes were ignored, the model is in good agreement with the experimental data. For example the predicted effect of flowrate on the current density distribution, shown in Fig. 10 as a normalized distribution, that is, local value divided by the average value for the cell, corresponds reasonably well to experimental data (see Fig. 7(d)). In the data the higher flowrates result in the smaller current densities at the cell inlet and highest current densities at the cell exit. However, this is not a satisfactory approximation for this type and size of electrochemical reactor, although for larger reactors with electrodes of greater length it becomes a better approximation.

The current density distributions exhibited in the DEM cell are quite similar to those obtained by Bisang [26] for a parallel plate cell with sulphite ion oxidation and hydrogen gas evolution. In the work of Bisang the electrolyte flow is laminar and the mass transfer distribution varies inversely with the square root of distance along the electrode for a single phase electrolyte. This distribution in mass transport produced fair agreement between model and experiment for the work of Bisang [26]. It might therefore be reasonable to assume that a similar distribution in mass transfer behaviour for the DEM cell would improve the agreement between model and experimental data. However the DEM cell utilizes a turbulence promoting mesh and thus it is preferable to measure the local variation in mass transport under conditions associated with the reactor operation.

6. Conclusions

Measurements of current density distribution in a DEM cell during the anodic oxidation of bromide solutions have shown significant distributions over the electrode surface. The current density varies both across and along the electrode and, typically, is higher at the electrolyte flow inlet and lower at the flow exit. The distribution in current density is particularly affected by the change in contour of the

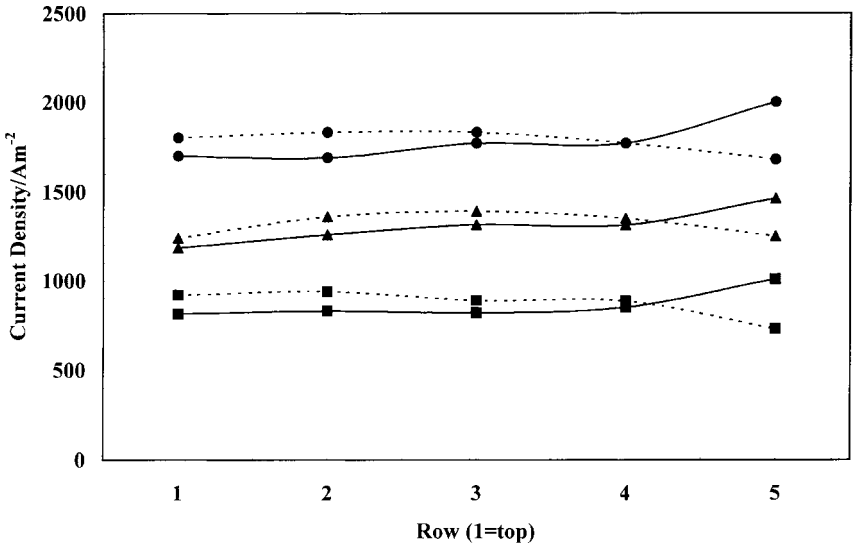

Fig. 9. Comparison of experimental and model predictions of current distribution (flowrate 298 cm^3 s^{-1}). Key: (■) 40 A, 1.0 M, (▼) 40 A, 1.5 M, (▲) 60 A, 1.0 M.

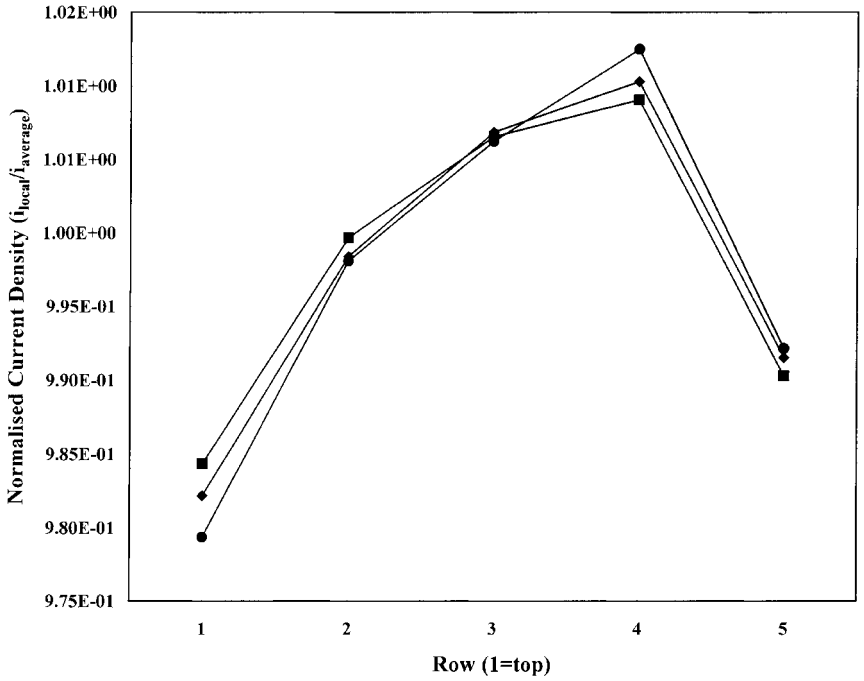

Fig. 10. Effect of flowrate on theoretical current distribution. 1.0 M KBr, 40 A. Flowrate/$cm^3 s^{-1}$: (◆) 100, (■) 110 and (●) 90.

dished electrode at the inlet, which influences mass transport, the potential field and possibly 'back-mixing' of evolved gas.

A one dimensional model of the current distribution, which has been used with some success for a parallel plate cell during sulphite ion anodic oxidation [26], does not give reasonable predictions of the overall current distributions in the DEM cell. This is due to several factors: (i) a lack of localized mass transfer data in the cell when a counter electrode gas evolution reaction occurs; (ii) the variation in the electric potential field at the edge of the electrodes, which is not allowed for in the model; and (iii) the distribution in flow, and consequently current density, vary in two dimensions in the cell.

Overall the relative complex flow behaviour which occurs in a DEM cell makes the actual performance for any synthesis difficult to predict. This flow behaviour changes on scale-up and thus mass transport and current density distribution will also change. This in part may explain why the performances of the DEM cell for the electrosynthesis of bromate changes on scale-up [27].

References

[1] H. Vogt, 'Gas Evolving Electrode' in 'Comprehensive Treatise of Electrochemistry', Vol. 6 (edited by E. Yeager, J. O'M. Bockris, B. E. Conway and S. Sarangapani), Plenum Press, New York (1983).
[2] W. S. Wu and G. P. Rangaiah, *J App. Electrochem.* **23** (1993) 1139.
[3] G. H. Sedahmed, *ibid.* **10** (1980) 351.
[4] A. M. Ahmed and G. H. Sedahmed, *J. Electrochem. Soc.* **135** (1988) 2766.
[5] K. Scott and B. Hayati, Symposium On Electrochemical Cell Design and Optimisation Procedures, Dechema, 24–26 Sept. (1990).
[6] H. Vogt, *Electrochim. Acta* **23** (1978) 203.
[7] C. I. Elsner and S.L. Maarchiano, *J. App. Electrochem.* **12** (1982) 735.
[8] L. J. J. Janssen, *ibid.* **17** (1987) 1177.
[9] H. Vogt, *ibid.* **19** (1989) 713.
[10] M. G. Fouad and G.H. Sedahmed, *Electrochim. Acta* **18** (1973) 55.
[11] L. J. J. Janssen and E. Barendrecht, *ibid.* **24** (1979) 693.
[12] M. F. Sherbiny, A.A. Zatout, M. Hussien and G. H. Sedahmed, *J. App. Electrochem.* **21** (1991) 537.
[13] O. N. Cavatorta, U. Böhm and A. M. Chiappori De Del Giorgio, *J. App. Electrochem.* **21** (1991) 40.
[14] P. J. Sides, 'Modern Aspects of Electrochemistry', No. 18 (edited by R. E. White), Plenum Press, New York (1986), p. 303.
[15] N. Ib1, *Electrochim. Acta* **24** (1979) 1105.
[16] L. Sigrist, O. Dossenbach and N. Ib1, *Int. J. Heat & Mass Transfer* **22** (1979) 1393.
[17] C. W. Tobias, *J. Electrochem. Soc.* **106** (1959) 833.
[18] J. E. Funk and J.F. Thorpe, *ibid.* **116** (1969) 48.
[19] Y. Nishiki, K. Aoki, K. Tokuda and H. Matsuda, *J. App. Electrochem.* **16** (1986) 615.
[20] I. Roušar, V. Cezner and J. Hostomsky, *Collect. Czech. Chem. Comm.* **36** (1971) 1.
[21] I. Roušar, V. Cezner, J. Nejepsova, M.M. Jackson, M. Spasojevie and B.Z. Nikolic, *J. App. Electrochem.* (1977) 427.
[22] I. Roušar, *J. Electrochem. Soc.* **116** (1969) 676.
[23] J. M. Bisang, *J. App. Electrochem.* **21** (1991) 760.
[24] L. J. J. Janssen and C. J. Visser, *ibid.* **21** (1991) 753.
[25] L. R. Czarnetzki and L. J. J. Janssen, *ibid.* **19** (1989) 630.
[26] J. M. Bisang, *ibid.* **23** (1993) 966.
[27] P. Millington and D. Blum, 'Electrosynthesis from Laboratory, to Pilot, to Production', (edited by J. D. Genders and D. Pletcher), The Electrosynthesis Co., New York (1990), chapter 12.
[28] K. Scott, 'Electrochemical Processes for Clean Technology', Royal Society of Chemistry, Cambridge, UK (1995).
[29] K. Scott, 'Electrochemical Engineering and Energy', (edited by F. Lapicque, A. Storck and A.A. Wragg), Plenum Press, London (1994), p. 141.
[30] P. Cettou, P. M. Robertson and N. Ibl, *Electrochim. Acta* **29** (1984) 875.
[31] W. Taama, 'Mass Transfer Studies in a DEM Electrochemical Cell' PhD thesis, University of Newcastle, UK (1991).
[32] D. J. Economou, MS thesis, University of Illinois, IL (1983).